Earthquake Scaling Equations Under Small Strain, Steady Moment Release-Rate Conditions in Southern Andes from 2015 to 2017

Patricio A. Toledo[1], Cristián Siegel[1,3], Benoit Derode[4], Raúl Madariaga[1,2], Jaime Campos[1,3]

[1]Programa de Riesgo Sísmico PRS, Universidad de Chile, Blanco Encalada 2002, Santiago, Chile.
[2]Département de Géologie, Ecole Normale Superieure, PSL University, 75005 Paris, France.
[3]Departamento de Geofísica, Facultad de Ciencias Físicas y Matemáticas, Universidad de Chile, Beauchef 850, Santiago, Chile.
[4]Institut de Recherche en Astrophysique et Planétologie, 14 Avenue Edouard Berlin, 31400 Toulouse, France.

Key Points:

- We derived a set of scaling equations linking renormalization variables for earthquake generation processes
- We found scaling laws valid across multiple orders of magnitude
- Analyzing statistical (seismic laws) imbrications highlights the importance of the method for large-scale earthquake hazard

Corresponding author: Cristián Siegel, `cristian.siegel@uchile.cl`

Abstract

In the South Andes western edge, a very active seismic contact, with earthquakes up to magnitude 9.5 and ca. 4000 km extension threatens cities and very large populations. The existence of modern seismological networks along the contact allowed the observation of unprecedented earthquake cycle characteristics, which can improve our ability to estimate earthquake hazard, a main objective of seismology. Using dimensional and similarity analysis techniques, we show precise mechanical conditions under which the earthquake generation process unfolds, and derive a set of scaling equations linking renormalized variables. Later on, we test our theoretical results using a curated earthquake point-catalog by using gridding, box-counting, statistical bootstrap and fixed-point iteration collapse techniques. We found non-trivial scaling laws valid across multiple orders of magnitude capable of describing a complex interplay between renormalized earthquake occurrence and renormalized moment release rate. We discuss finite-strain and seismic-moment release-rate conditions; declustering, foreshock, mainshock, aftershock notions; cutoff magnitudes, earthquake hazard implications and a possible large-scale tectonic energy transfer mechanism.

Plain Language Summary

Earthquakes are the most destructive natural hazard affecting the western edge of South America. If precise earthquake generation conditions are known, then effective public policies might be put in place. In this work, we review practical issues and theoretical aspects of the earthquake generation process and we propose simple relationships between the observable variables at world-wide Seismological Centers. This relationships might be used by decision takers and other scientists as well to advance societal well-being.

1 Introduction

At the western edge of South America two plates subduct, the Nazca Plate to the north and the Antarctic Plate to the south (Ranero et al., 2006). This configuration defines the Southern Andes as one of the seismic zones with the greatest extension and seismic activity, far exceeding 4000 km long, where earthquakes up to magnitude 9.5 (Ruiz & Madariaga, 2018) have been recorded. In Chile, this condition directly affects large communities. For instance Camus et al. (2016) estimated in 11 million the affected population in 2010 only. Therefore, knowing the behavior of seismicity presents a fundamental scientific challenge, and at the same time a practical public policy issue. The precise determination of statistical laws and conditions under which the earthquake generation process unfolds requires theory and experimental observations with positive implications in earthquake hazard analysis. Taking advantage of the unique opportunity that this geographic area represents, during the last decades large instrumental network-installation and maintenance efforts have been made, that have made possible to build earthquake point-catalogs allowing exploration of previously unobserved properties. Therefore, it is expected that these new observations will lead to new extended laws that will improve our understanding of the processes occurring in the crust, and ultimately improve our ability to estimate earthquake hazard.

Our paper is organized as follows: In Section 2 we describe the problem of seismicity generation framed in a seismic-moment loading-unloading cycle. Then we describe precise conditions, based on observations, to simplify the problem and make the main similarity assumptions. Section 3 describes the scaling equations describing the cycle. This set of equations represent the correlations developed as the seismicity phenomenon unfolds. Section 4 presents a review of the tectonic context in which the scaling equations are intended to be applied, and describes the existing instrumentation and data set. Subsequently, the main methodological and statistical elements used to process the

earthquake point-catalog information are indicated. In Section 5 the results are presented and the main scaling characteristics describing the existing correlations are shown. Finally, in Section 6, the implications are reviewed and discussed.

2 Problem setting

As the Earth crust is the place where the earthquake generation process takes place, let us consider a region $\mathcal{R}$ (Figure 1) where the main elements in consideration are set. Let us parameterize the crust by considering the class of systems of units ELT, where units of energy, length and time are used to describe the quantities of interest. We suppose that the crust is characterized by a seismogenic thickness H. A certain power R — the main source of available energy— is injected into the crust from the heat flux through Earth mantle and it is applied at ocean expansion rifts over a very long time T, as a tectonic loading process. A fraction Q of the inyected power R is freed when crust-faults slip a certain amount u releasing a stress-drop $\Delta\sigma$, producing earthquakes whose sizes are measured through a scalar seismic-moment Mo. Therefore Q represents a seismic-moment release rate. In general Q is different from R, inducing a proper interevent time distribution $\tau = Mo/R$, associated with earthquake recurrence phenomena, which can be consecutive events located in the same place (first-return events) or scattered events separated at a distance ℓ within the region bounds (all-return events).

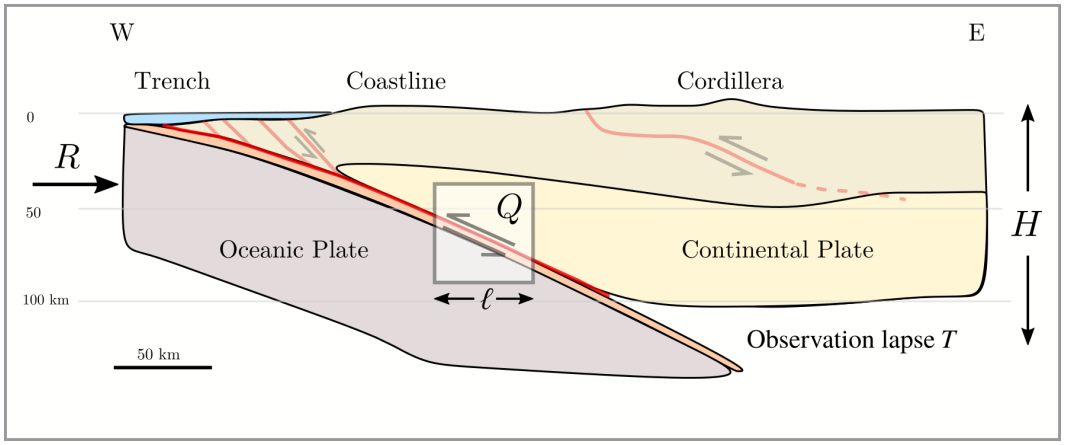

Figure 1. Cross section sketch of a subduction border. An energy injection is placed west with a power R, feeding a complex tectonic process with characteristic geomorphologies (trench, coastline and cordillera) induced by a Continental Plate overriding an Oceanic Plate. Within a volume with proper-length ℓ, a release process Q takes place across a larger volume with proper-length H. The observation period T determines the longer time periods available for study.

Therefore, as a hazard approximation, we wish to estimate the number of events per unit time and unit area n taking place in the given geographic region of interest $\mathcal{R}$, during the observation period T given by a general relation φ linking n and the aforesaid parameters:

$$n = \varphi\left(\ell, \tau, \Delta\sigma, T, Mo, H, u, Q\right). \tag{1}$$

Table 1 shows powers of the dimension function for each parameter, for instance, the dimensions of the number of events distribution are $[n] = \mathrm{L}^{-2}\,\mathrm{T}^{-1}$, the dimensions of the stress-drop are $[\Delta\sigma] = \mathrm{E}\,\mathrm{L}^{-3}$, the dimension of the interevent distance is $[\ell] = \mathrm{L}$, and the dimension of the interevent time is $[\tau] = \mathrm{T}$.

Table 1. Powers of the dimension function in the ELT class for each parameter used in text.

	n	ℓ	τ	$\Delta\sigma$	T	Mo	H	u	Q
E	0	0	0	1	0	1	0	0	1
L	−2	1	0	−3	0	0	1	1	0
T	−1	0	1	0	1	0	0	0	−1

Thus, the number of events distribution n is a function of 8 parameters. As ELT has 3 independent units, there are 3 quantities with dimensions that might be considered independent, let us choose $\Delta\sigma, \ell$ and τ. Therefore, there are $m = 5$ parameters with dependent dimensions. According to dimensional analysis (Sedov, 1993) a function Φ exists such that:

$$\frac{n}{\ell^{-2}\tau^{-1}} = \Phi\left(\frac{T}{\tau}, \frac{Mo}{\Delta\sigma\ell^3}, \frac{H}{\ell}, \frac{u}{\ell}, \frac{Q}{\Delta\sigma\ell^3\tau^{-1}}\right), \tag{2}$$

which is a general result obtained from units alone. In mathematical terms, Φ is symmetric with respect to a group of transformations defining change from one system of units to another within a given class of systems of units. In physical terms, meaningful laws cannot depend on the choice of units, therefore it must be possible to express them using relationships between quantities that do not depend on this arbitrary choice, i.e. dimensionless combinations of variables.

Let us introduce the dimensionless quantities:

$$\Pi = \frac{n}{\ell^{-2}\tau^{-1}}, \quad \Pi_T = \tfrac{T}{\tau}, \quad \Pi_{Mo} = \frac{Mo}{\Delta\sigma\ell^3},$$
$$\Pi_H = \frac{H}{\ell}, \quad \Pi_u = \tfrac{u}{\ell}, \quad \Pi_Q = \frac{Q}{\Delta\sigma\ell^3\tau^{-1}},$$

The relation (2) might then be expressed as follows:

$$\Pi = \Phi\left(\Pi_T, \Pi_{Mo}, \Pi_H, \Pi_u, \Pi_Q\right), \tag{3}$$

If we would like to obtain the earthquake occurrence probability distribution, that is to say to sample the distribution Π, we should explore a space of 5 dimensions, one for each dimensionless quantity. If we consider 10 independent observations to estimate the expected value of these dimensionless quantities, we get that an earthquake point-catalog should have at least 10^5 observations, reasonable smaller than 10^8 elements of the original formulation in equation (1).

2.1 Complete similarity conditions

On a physical level a parameter is considered essential, i.e. governing the phenomenon, if the value of the corresponding dimensionless parameter is not too large or not too small (about 0.1 and 10). Thus, let $l \leq m$ define a subset of the parameters. If the dimensionless parameters $\Pi_{l+1}, \ldots, \Pi_m$ are small or large, it is assumed by convention that the influence of these dimensionless parameters, and consequently of the corresponding dimensional parameters, can be neglected (for a discussion and theorems sustaining this procedure see Barenblatt, 2003). If these conditions are actually satisfied for sufficiently small or sufficiently large $\Pi_{l+1}, \ldots, \Pi_m$ the function $\Phi(\Pi_1, \ldots, \Pi_l, \Pi_{l+1}, \ldots, \Pi_m)$ can be replaced by a function Φ^* with fewer arguments:

$$\Pi = \Phi^*\left(\Pi_1, \ldots, \Pi_l\right). \tag{4}$$

In such cases, we speak of *complete similarity* or *similarity of the first kind* of a phenomenon in the parameters $\Pi_{l+1}, \ldots, \Pi_m$(Barenblatt, 1987).

The observational period T and the interevent times τ define Π_T which is the inverse of Deborah number De, used in very-short or very-long term rheology experiments (Huilgol & Phan-Thien, 1997; Mendecki, 1996). Deborah number is the ratio between the characteristic relaxation (response) time of a body subjected to a load, and the process loading-time duration itself, thus for $De \ll 1$ the body behaves like a liquid and for $De \gg 1$ like a solid. The parameter Π_T poses a very common problem in seismology and geodesy, while the tectonic energy-dissipation process spans millions of years, modern earthquake point-catalogs are decades long (Mueller, 2019). Although historical data might increase the period to hundreds of years (Lomnitz, 1970, 2004; Udías et al., 2012) and paleoseismology to thousands (Cisternas et al., 2012; Vargas et al., 2014) in most scenarios Π_T is very large. In practice, for an open period we cannot know, a priori, which events have interevent times smaller than the observation period, at least for causal phenomena. This parameter cannot be neglected.

The dimensionless parameter Π_{Mo} is discussed (at length) by Golitsyn (2007, 2001). The factor $Mo/\Delta\sigma$ represents, according to Tsuboi (1940, 1956), a volume where seismicity takes place. Thus, every earthquake is endowed with a proper-length scale $\sqrt[3]{Mo/\Delta\sigma}$ (Aki, 1972; Kostrov, 1974). It has been known for a while the remarkable low fluctuations of $\Delta\sigma$, and various scaling laws can be derived from this observation (Kanamori & Anderson, 1975; Aki, 1967). A common value for stress-drop is $\Delta\sigma \simeq 4\,\mathrm{MPa}$ (Allmann & Shearer, 2009), thus if stress-drop is nearly constant, then the seismic-moment should scale with the cube of this length scale (Madariaga, 1979) and Π_{Mo} is expected to fluctuate heavily in earthquake point-catalog surveys, and then cannot be neglected.

The parameter Π_H plays a role similar to Knudsen Kn number in statistical physics (Rapp, 2016). It is the ratio of seismogenic thickness H controlling the spatial region of interest and the interevent distance ℓ. For most earthquake pairs ℓ will be small compared to H, so Π_H should be very large, but long-range space correlations (Kagan & Knopoff, 1980) implies that a considerable number of earthquake pairs will have interevent distances comparable with the seismogenic thickness, therefore Π_H remains essential (Aki, 1996) and cannot be neglected.

The dimensionless parameter Π_Q represents the seismic-moment release-rate process. On the global scale Q was estimated to be around $1.2{\times}10^{13}\,\mathrm{W}$ (Golitsyn, 2001). The parameter Q governs the earthquake load-release cycle. The product τQ might be interpreted as the seismic-moment released at the time scale τ whereas the product τR represents the injected energy at the same time period. Thus the ratio R/Q might be interpreted as the balance between crustal work inducing loading and crustal work inducing release, the energy budget responsible for the seismic cycle should display a deficit if $R/Q < 1$ and equilibrium if $R = Q$ and a surplus otherwise. Precise earthquake point-catalogs should display fluctuations in Π_Q and cannot be neglected.

The fault slip u is a parameter that scales with the seismic-moment with a power-law (Aki, 1972) thus Π_u is not expected to be constant, but as long as the interevent distance ℓ remains long enough compared with fault slip, this parameter, that represents a finite strain, will be small. It is therefore natural to introduce a *first similarity hypothesis* regarding small finite strains and propose a further simplification of equation (3):

$$\Pi = \Phi^* \left(\Pi_T, \Pi_{Mo}, \Pi_H, \Pi_Q\right), \tag{5}$$

i.e. based on observational facts, we claim there is complete similarity in the parameter Π_u. We expect therefore the function Φ to converge —fast enough— to a non-zero limit Φ^* when the aforementioned dimensionless quantity goes to zero.

2.2 Incomplete similarity conditions

The situation just described is far from being the general case. According to Barenblatt (2003) when the dimensionless parameters $\Pi_{l+1}, \ldots, \Pi_m$ go to zero or infinity the func-

tion Φ does not necessarily tends to a limit. Therefore, the physical parameters remain essential, no matter how small or large the values of the corresponding dimensionless parameters $\Pi_{l+1}, \ldots, \Pi_m$ are. It just happens that there exists another class of phenomena, wider that the class of *complete similarity* phenomena, where the function Φ have at large or small values of $\Pi_{l+1}, \ldots, \Pi_m$ the property of generalized homogeneity in its own dimensionless arguments:

$$\Phi = \Pi_{l+1}^{\alpha_{l+1}} \cdots \Pi_m^{\alpha_m} \Phi^* \left(\frac{\Pi_1}{\Pi_{l+1}^{\beta_1} \cdots \Pi_m^{\delta_1}}, \ldots, \frac{\Pi_l}{\Pi_{l+1}^{\beta_l} \cdots \Pi_m^{\delta_l}} \right), \tag{6}$$

where $\alpha_{l+1}, \ldots, \alpha_m, \beta_1, \ldots, \delta_l$ are unknown exponents. We remind that equation (3) comes from (group) covariance of meaningful physical laws under units change, on the other hand the generalized homogeneity of equation (6) is a particular property. The exponents cannot be obtained, even in principle, by dimensional considerations, i.e. they are not universal and they depend on specific conditions of the problem under study. The parameters $\Pi_{l+1}, \ldots, \Pi_m$ —which are violating complete similarity— do not disappear from the analysis, they continue to remain essential, no matter how large or small its similarity parameters are. We say the solutions *scale* with the dimensionless quantities $\Pi_{l+1}, \ldots, \Pi_m$. As proposed by Zel'dovich (1956), in such cases we speak of *incomplete similarity* or *similarity of the second kind* in the relevant parameter. Often, the exponents are obtained by fitting experimental results, observations, or by numerical modeling. They tend to be real non-rational values, physicists call these exponents *anomalous dimensions* (Wilson, 1975, 1979) and the scaling procedure bears the name *renormalization* (Kadanoff, 1966) which is a by-product of covariance of Φ^* under rescaling of its own dimensionless arguments (Goldenfeld, 1992).

Beginning with the work of Bak et al. (2002); Christensen et al. (2002) and the precursory research of Kossobokov and Mazhkenov (1994) a systematic generalization of earthquake scaling relations took place. It is now recognized that a wider set of laws rule the seismic-moment release-rate process in the crust (Corral, 2003). Equation (5) expresses earthquake occurrence statistics under very restricted (complete) similarity conditions. Extensive observational data describing long-period interevent time correlations (Omori, 1894; Utsu et al., 1995; Ogata, 1988) suggests that there is incomplete similarity in the parameter Π_T under conditions of large (and small) values of the dimensionless parameter, that is:

$$\Pi = \Pi_T^{\alpha} \Phi^* \left(\frac{\Pi_{Mo}}{\Pi_T^{\alpha_{Mo}}}, \frac{\Pi_H}{\Pi_T^{\alpha_H}}, \frac{\Pi_Q}{\Pi_T^{\alpha_Q}} \right), \tag{7}$$

where $\alpha, \alpha_{Mo}, \alpha_H$ and α_Q are real-valued exponents. Analogous conditions over seismic-moment dimensionless parameter Π_{Mo} are well known (Gutenberg & Richter, 1956):

$$\Pi = \Pi_T^{\alpha} \Pi_{Mo}^{\beta} \Phi^* \left(\frac{\Pi_H}{\Pi_T^{\alpha_H} \Pi_{Mo}^{\beta_H}}, \frac{\Pi_Q}{\Pi_T^{\alpha_Q} \Pi_{Mo}^{\beta_Q}} \right), \tag{8}$$

where β, β_H, and β_Q are real-valued exponents also. Similar evidence regarding long-range interevent distance correlations (Kagan & Knopoff, 1980; Scholz & Aviles, 1986; Okubo & Aki, 1987), as well as (renormalization) group symmetries (Corral, 2005) suggests that under conditions of large (or small) values of the similarity parameter Π_H, incomplete similarity exists, that is:

$$\Pi = \Pi_T^{\alpha} \Pi_{Mo}^{\beta} \Pi_H^{\gamma} \Phi^* \left(\frac{\Pi_Q}{\Pi_T^{\alpha_Q} \Pi_{Mo}^{\beta_Q} \Pi_H^{\gamma_Q}} \right), \tag{9}$$

with γ and γ_Q real-valued exponents. Rearranging terms, a symmetrical form might be obtained that can be interpreted in terms of renormalized parameters only:

$$\Pi^* = \Phi^*(\Pi_Q^*), \tag{10}$$

where Π^* is the renormalized event number and Π^*_Q is the renormalized seismic-moment release-rate number. Thus, the equation (10) represents a *second similarity hypothesis*, regarding long-range correlation conditions. We must remark that exponents $\alpha, \beta, \gamma, \alpha_Q, \beta_Q$, and γ_Q define the number of events distribution given the particular seismic conditions (interevent times, interevent distances, seismic-moment, seismic-moment release-rate), tectonic conditions (stress-drop and seismogenic width) and other region-dependant parameters (observation period). Note that constancy of Q lead us to a hypothesis regarding steady seismic-moment release-rate conditions.

3 Scaling equations

Going back to the original variables in equation (10) we might write:

$$n\tau^p Mo^b \ell^d = f(\tau^{p_Q} Mo^{b_Q} \ell^{d_Q}), \tag{11}$$

where f is a scaling function depending on tectonic conditions at play. Moreover, a set of relationships between the unknown exponents associated with renormalization group symmetries and exponents associated with the physical parameters might be obtained:

$$\left\{ \begin{array}{rclrclrcl} p & = & \alpha + 1, & b & = & -\beta, & d & = & 3\beta + \gamma + 2, \\ p_Q & = & \alpha_Q + 1, & b_Q & = & -\beta_Q, & d_Q & = & 3\beta_Q + \gamma_Q - 3. \end{array} \right. \tag{12}$$

This conditions are termed scaling relations, and represent fundamental objects in critical phenomena theory (Widom, 2009). The exponent p is related to Omori law, d is related to epicenters fractal dimension and b is related to seismic moment scaling. When Φ^* is linear, exponents p_Q, d_Q and b_Q are reduced to Omori, Gutenberg-Richter and fractal laws. Power law behavior is a very special case, and tapered exponential has long been advocated (Kagan, 1994). By inspection of (12) it can be said that interevent-times exponents are independent in contrast to interevent-distances and seismic-moment release-rate exponents, which are always related. Note that while p should be positive (negative) so that a decay (increase) in events number follows increasing (decreasing) interevent times, b and d are more complex. Aki (1981) stated two scenarios for faults: linear objects filling a surface ($1 < d < 2$), or planar objects filling a volume ($2 < d < 3$). Working on disordered materials Carpinteri and Chiaia (1997) suggested two scenarios in fatigue cycles, a loading process defined over lacunar (Cantor-like) sets where progressive void-appearance speeds-up failure by stress concentration, and a release process defined over invasive (Koch-like) sets where progressive detail-appearance speeds-up dissipation by surface-energy build-up. As seen in Figure 2 there is ample space for those scenarios depending on γ values. For instance, if $\gamma = -1$ then invasive sets with dimension $d < 1$ support moment distributions as long as $b \leq 1/3$. On the contrary lacunar sets occur for $b > 1/3$, and values of $\gamma = -2$ are always associated with lacunar sets, as long as $b > 0$.

4 Southern Andes tectonic framework, data and statistical techniques

As shown in Figure 3a Nazca plate advances at $68\,\mathrm{mm\,y^{-1}}$ (Norabuena et al., 1998) in N76E direction (Angermann et al., 1999) with respect to South America, forming a convergent contact. The trace of convergence (trench) is roughly aligned NS at the greater bathymetric depths. Under the continent, the northern subducting plate segment shows a simple but abrupt morphology up until 33°S (Contreras-Reyes et al., 2012), correlating with a tectonic erosive regime along the overriding plate base. The southern segment shows a flattened subduction plate and a tectonic accretionary border that reaches up until 45°S where an erosive regime develops again. Further south, the Pacific Plate subduces South America at $18\,\mathrm{mm\,y^{-1}}$ under accretionary conditions not fully understood yet (Ranero et al., 2006). The volcanic arc (mostly) follows the aforementioned tectonic regimes with active volcanoes distributed along the Andes with a sharp gap between 30

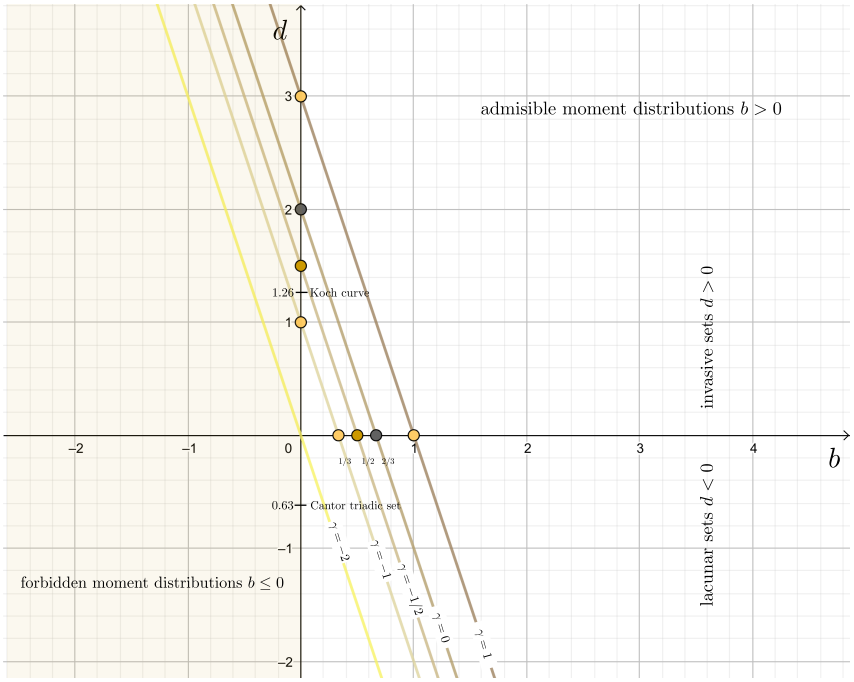

Figure 2. Scaling laws representing the relationship between b and d for various values of γ. Admissible values for b are positive, while d values can be positive (invasive sets) or negative (lacunar sets). Laws with $\gamma \leq -2$ always represent lacunar sets for b positive, laws with $-2 \leq \gamma \leq -1$ represent lacunar sets for $b \leq 1/3$ and invasive sets for $b > 1/3$. Fractal dimensions for Koch curve and Cantor triadic set are shown as reference.

and 35°S (Ranero et al., 2006). From 2001 onwards various earthquakes with magnitudes greater than 7.0 have been recorded. Northern notable earthquakes are the 2005 *Mw* 7.8 Tarapacá earthquake, the 2007 *Mw* 7.8 Tocopilla earthquake, the 2007 *Mw* 7.7 Iquique earthquake and the great 2014 *Mw* 8.2 Iquique earthquake. Central South Andes has not presented earthquakes greater than 6 after 2001, but extensive swarms have been recorded. Southern notable earthquake are 2001 *Mw* 7.0 Papudo earthquake, the great 2010 *Mw* 8.8 Maule earthquake, the 2011 *Mw* 7.1 Arauco earthquake, the great 2015 *Mw* 8.3 Illapel earthquake and the 2016 *Mw* 7.6 Chiloé earthquake. A thorough description of these events can be found in Ruiz and Madariaga (2018). Figure 3b shows the station network managed by the Plate Boundary Observatory (IPOC), Geoscope, the Global Seismograph Network (GSN) and the Chilean National Seismological Center (CSN). A variety of instruments compose the network. Derode et al. (2019) reports the use of modern broadband and accelerometers distributed across the western South Andes border. Thus, there is spatial covering homogeneity but heterogeneous instrumental capacity. In Figure 3c the earthquake point-catalog used in this study is shown, where 6274 earthquakes were analyzed with FMNEAR method (Delouis, 2014) from January 1st, 2015 until December 31, 2017. Earthquake hypocenters with shallow depth near the trench represent ca. 60% of the catalog whereas 30% are intermediate-depth events (> 70 km), occurring mostly north of 25°S latitude, with prominence between 19 and 23°S. Maximum estimated earthquake depth is 390 km while magnitudes range between *Mw* 1.7 and 7.8, (see Derode et al., 2019, for further details).

The main data analysis tool is the gridding and box-counting technique (Feder, 2013) as shown in Figure 4, right panel. The region $\mathcal{R}$ is covered by a bidimensional grid $\mathcal{G}^\ell$ composed of proper-length ℓ cells $\mathcal{G}^\ell_{ij}$, where $i, j = 1, 2, \ldots$ are positional indices. The

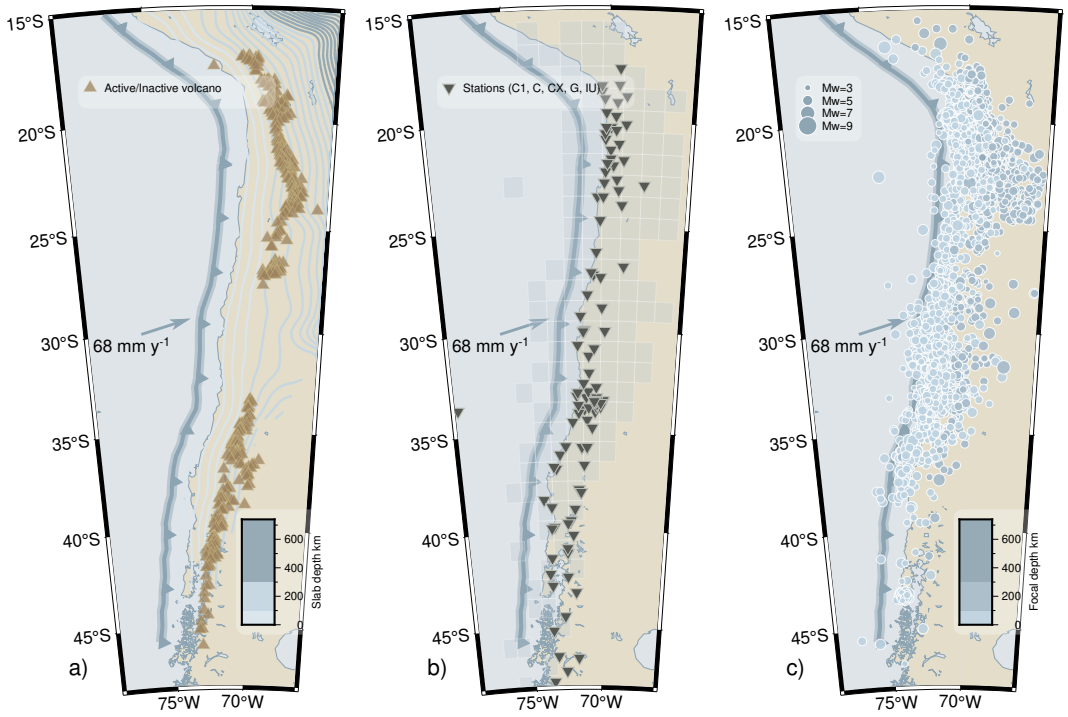

Figure 3. Tectonic, network and earthquake point-catalog context. Left a) plane view of western South America. The subduction trace (trench) is roughly axial to coast line. The Nazca plate advances at $68\,\mathrm{mm\,y^{-1}}$ long-term velocity. A volcanic arc appears parallel to coastline with a remarkable gap correlated with a flatter subduction interface (colored isobath lines). Center b) The seismic network being operated, also a grid with cells covering the region of interest. Right c) Seismicity during 2015-2017 period as published by (Derode et al., 2019).

intersection of an earthquake point-catalog $\mathcal{C}$ with $\mathcal{G}^\ell$ generates subcatalogs $\mathcal{C}_{ij}^\ell$ as illustrated in Figure 4, left panel. These subcatalogs represent a deformation field which is a mathematical object that might be described by a punctuated random-field process, with earthquakes acting as points scattered at a distances always shorter than ℓ within $\mathcal{G}_{ij}^\ell$. To ensure small finite strain conditions a cutoff must be imposed on every event in every subcatalog. We built the cells matching the typical earthquake source radius $r^3 = \frac{7}{16}\frac{Mo}{\Delta\sigma}$ from Madariaga (2020) and we selected only those events with estimated radius smaller than cell proper-length ℓ, under these conditions Π_u is small and the first similarity hypothesis is always fulfilled.

Table 2. Grid characteristics used in the study, see Figure 4 and Figure 3b.

	$\mathcal{G}^\ell$					
Cell Length ℓ, km	3	10	33	100	333	1000
Magnitude cutoff	5	6	7	8	9	10
Min return period, s	3.59×10^3	2.87×10^3	1.02×10^5	4.60×10^5	8.11×10^5	1.46×10^6
Max return period, s	9.24×10^7	9.37×10^7	9.40×10^7	9.46×10^7	9.46×10^7	9.46×10^7
Number of cells	4848	2498	688	154	29	4

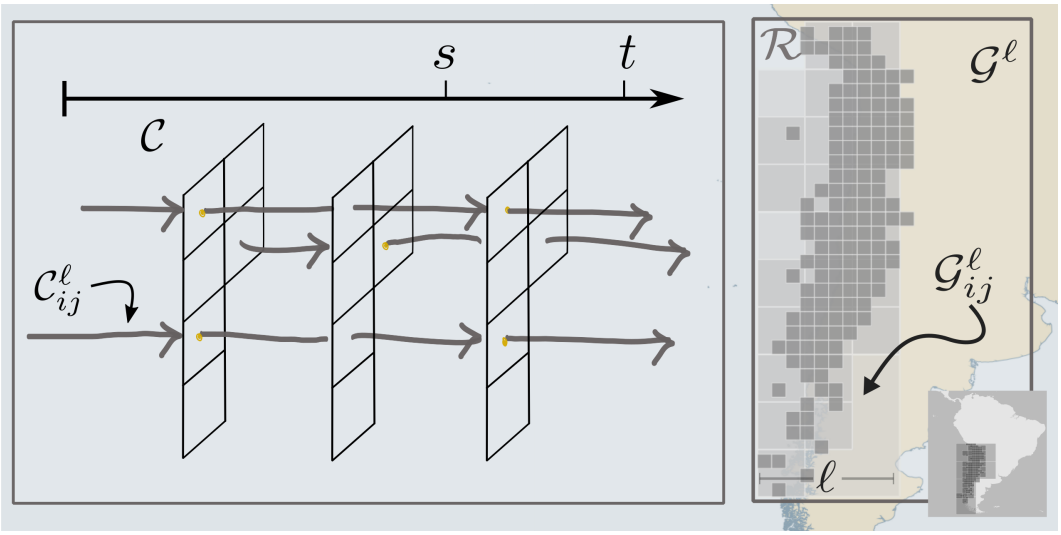

Figure 4. Earthquake point-catalog sketch and gridding-technique. An earthquake point-catalog might be intersected with a grid $\mathcal{G}^{\ell}$ covering a region $\mathcal{R}$. An evolution process marked at specific points in time s and t where earthquakes occur is induced, thereby creating a subcatalog $\mathcal{C}_{ij}^{\ell}$ for every cell $\mathcal{G}_{ij}^{\ell}$ within the grid. As different proper scales ℓ are explored, the process precise description changes.

We used 6 grids, having cell (edge) proper-lengths between 3–1000 km, see Table 2 for specific characteristics. The grid with cells ca. 100 km proper-length is shown in Figure 3 b. For every subcatalog $\mathcal{C}_{ij}^{\ell}$ the governing parameters seismic-moment released *Mo*, interevent distances ℓ and interevent times τ are analyzed. Statistical estimators collected at every scale are cell maximal seismic-moment, cell maximal interevent distances and cell average interevent times (see tabulated statistics in Toledo et al., 2023). We must remark that average interevent times coincides with homogeneous Poisson process unbiased maximum-likelihood rate estimator, thus subcatalogs with 4 events or more are retained, although only 3 points minimum a required by theory.

This choice of maximal bounds avoids the use of binned density histograms, therefore we obtain cumulative experimental histograms which are more stable than density statistics known as source of problems in power law data (Virkar & Clauset, 2014) and also smears a known bias when fitting logarithmic data with least squares (Goldstein et al., 2004). Note that Gutenberg-Richter balance exponent b_{GR} is defined with respect to survival (complementary cumulative) magnitudes (Serra & Corral, 2017), and as we collect cumulative seismic-moments, we have $b = \frac{2}{3} b_{\mathrm{GR}}$. Also note that cumulative experimental histograms avoids $1 + \beta$ exponents that are source of confusions (Kagan, 1994).

The scaling function Φ^* in equation (11) is unknown, and supposing a power law translate the problem to a careful exponent estimation using constrained optimization fit (Branch et al., 1999). From a seed around expected exponents, 2500 iterations are produced each time sampling 25% of the data, so that mean values with 2σ reverse bootstrap percentile intervals (Diaconis & Efron, 1983; Efron & Tibshirani, 1994) are reported. We understand this fitting process as a collapse procedure —that is fixed point iterations using the renormalization group— in search for the special situation where all data fall-in a single curve that represents a stable point in the parametric space see Houdayer and Hartmann (2004).

Table 3. Scaling exponents as shown in Figure 6 and 5. Referential seismogenic thickness $H = 1.00 \times 10^5$ m, observation period $T = 9.46 \times 10^7$ s (3 years) stress-drop $\Delta\sigma = 4.00 \times 10^6$ Pa, and seismic-moment release-rate $Q = 1.00 \times 10^{12}$ W.

	α	β	γ	α_Q	β_Q	γ_Q
theory†	$+0.1$	$-\frac{2}{3}$	-2	$+0.1$	$+\frac{2}{3}$	$+3$
uncollapsed•	-0.7	-0.1	-2.5	$+0.9$	$+0.1$	$+3.5$
collapsed‡	$+0.09050^{+0.00009}_{-0.00014}$	-0.66	$-1.99063^{+0.00014}_{-0.00016}$	$0.10952^{+0.00009}_{-0.00013}$	0.99	$3.99063^{-0.00014}_{+0.00012}$

† See β values in Kagan (1994), α fits $p \simeq 1$ and γ a non-fractal surface. ‡ this study, • non physical.

Finally, a consideration is to be made regarding fractal dimension. In this case the calculated exponents corresponds to bidimensional box-counting dimension d_{BC}, which is an upper limit for Hausdorff dimension d_{H} (Ott, 2002), therefore $d_{\mathrm{H}} \leq d_{\mathrm{BC}}$.

5 Results

First order statistics are shown in Table 2. There are 6 grids with cell proper-lengths $3, 10, 33, 100, 333$ and 1000 km, the number of cells decrease from 4848 at proper-length 3 km to 4 at proper-length 1000 km, representing a lacunar fractal with dimension 1.24. The grid with proper-length 3 km, i.e. containing events with interevent distances ℓ no greater that 3 km and cutoff *Mw* 5, show average interevent return times τ from 3.59×10^3 s to 9.24×10^7 s, a range from minutes to years. The grid with cell proper-length 10 km shows the same long-period range. The grid with cell proper-length 33 km show an interevent return times range from 1.02×10^5 s to 9.40×10^7 s, a range from days to years. Grids with proper-lengths 100 and 333 km show the same long-period range. Finally the grid with proper-length 1000 km, cover the study area with 4 cells, have minimun average return period of 1.46×10^6 s and maximum average return period 9.46×10^7 s, a range from weeks to years.

In Figures 5 and 6 the collapse process is show. The situation in Figure 5 is not physically admisible. Very low γ and β (see exponents in Table 3) values are translated into a global trend with renormalized event number Π^* decreasing with renormalized seismic-moment release-rate Π^*_Q. Interevent return times τ (color encoded) display a inverse trend, same with interevent distances ℓ (symbol encode). But note the splitting pattern where different symbols do not mix at mid to lower Π^*_Q values, meaning that no unique scaling function Φ^* can describe the situation. Also note that for each symbol (each length scale ℓ) a corner can be seen, meaning that this particular set of exponents is not able to describe the renormalized event distribution within its boundaries. In Figure 6 a different situation is shown. A single inverse relationship between Π^*_Q and Π^* is displayed. There is considerable scatter, but a general trend where data from all scales involved collapse. As expected from a stable point, seismic-moment β exponent do not display appreciable variance to be reported, as seen in Table 3. Likewise α and γ also present small variability and both of them show a slight positive-skewness. The low p-value is consistent with our selection of (Poisson) interevent times estimator, moreover there are remarkable long-period correlations as seen in the strong overlapping.

Considering the large catalog extent, scaling exponents should be taken as averaged values, as fluctuations are present when considering each grid alone. These exponents are not crust parameters, they depend on the problem at hand, including its boundary conditions, so that specific places with different values are perfectly possible. A single scaling function Φ^*, fitting data across Southern Andes, with power-law shape might be proposed, but we do not rule out a tapered or other scaling laws. Indeed, a gentler

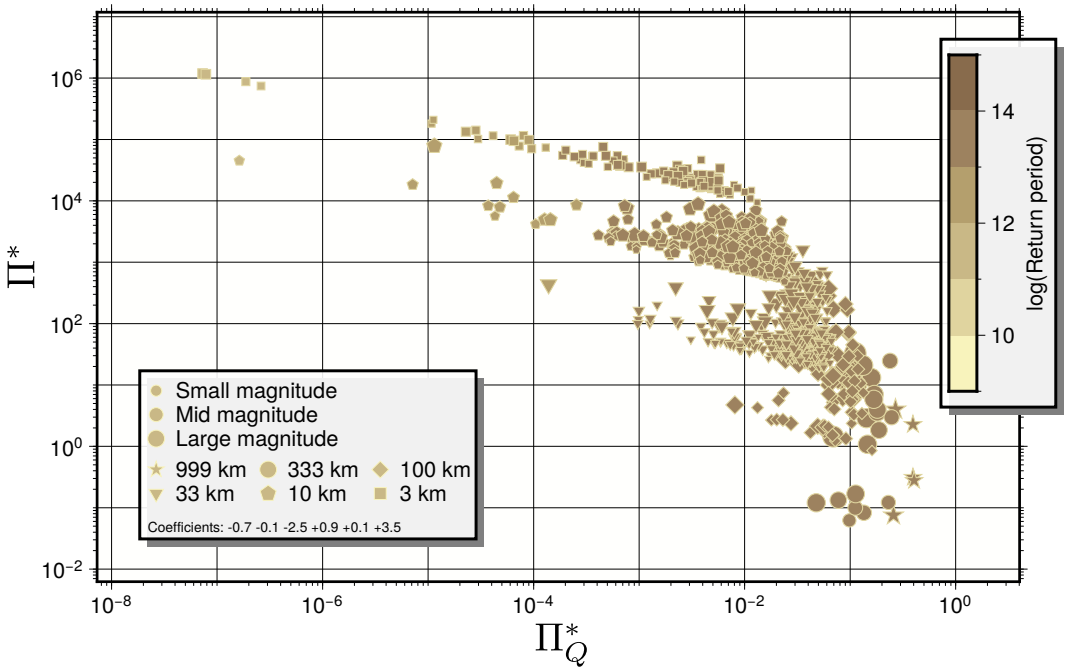

Figure 5. Uncollapsed scaling situation. Renormalized event number Π^* decrease with renormalized seismic-moment release-rate Π^*_Q. Note the clear splitting with interevent length ℓ, meaning that no scaling function Φ^* can describe the situation, and also note that for each curve a corner might be identified in Π^*_Q axis, meaning that this set of exponents is not able to describe the renormalized event distribution. Exponents as shown in Table 3. Referential seismogenic thickness $H = 1.00 \times 10^5$ m, observation period $T = 9.46 \times 10^7$ s (3 years) stress-drop $\Delta\sigma = 4.00 \times 10^6$ Pa, and seismic-moment release-rate $Q = 1.00 \times 10^{12}$ W.

slope might be seen at renormalized seismic-moment release-rates around $\Pi^*_Q \simeq 1$, meaning that complex structures are still hidden.

6 Discussion and conclusions

Similarity hypothesis. Considering the first similarity hypothesis about small-strain condition over Π_u, i.e. the condition on fault-displacements smaller than the proper scale ℓ, it might be said that there exists a prominent asymptotic (complete) similar solution as seen in the collapse reached by the curves indexed by ℓ. Further analysis will require a catalog with variables regarding processes with scales smaller than ℓ, that is the information from the physics at the seismic source. Considering the second similarity hypothesis, confirmed in view of the large dynamical range achieved by the renormalized parameters with a single set of exponents fitting a reasonably well behaved function Φ^*. Other earthquake point-catalogs, with longer observational periods, larger magnitude ranges and longer interevent-distances, should be studied to further confirm this hypothesis. Regarding the steady seismic-moment release-rate condition over Π_Q we can repeat the last argument. However, as suggested by Benzi et al. (2022), a steady seismic-moment release-rate is a variable affecting interevent time distributions, to further explore it we should relax the conditions over Π_Q and put back the injection rate R into the formulation, thus a catalog describing slow phenomena is then needed.

Griding and box-counting technique. Two main consequences might be extracted: 1) The natural declustering process taking place when dimensionless interevent-distances

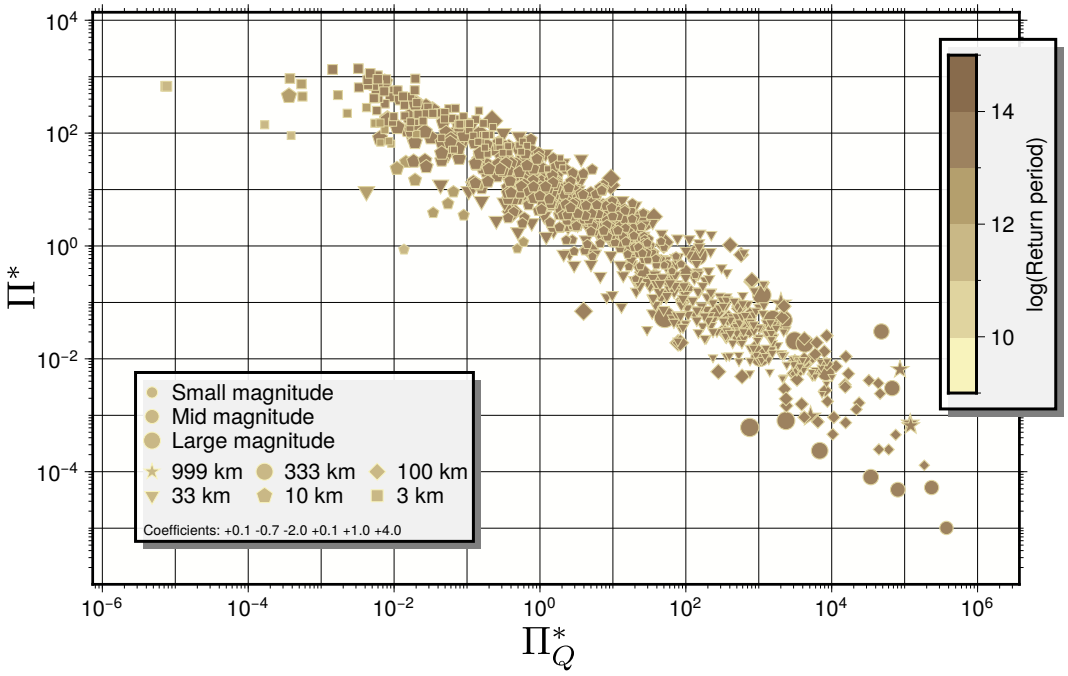

Figure 6. Collapsed scaling situation. Note the transition from gentler to steeper slopes near $\Pi^*_Q \simeq 1$, and also the nice collapsing across 10 orders of magnitude with strong overlapping, which is critical in earthquake hazard estimation. Exponents as shown in Table 3. Referential seismogenic thickness $H = 1.00 \times 10^5$ m, observation period $T = 9.46 \times 10^7$ s (3 years) stress-drop $\Delta\sigma = 4.00 \times 10^6$ Pa, and seismic-moment release-rate $Q = 1.00 \times 10^{12}$ W.

are considered. As there is no complete similarity in Π_H, the long-range correlations between event distances never disappear, so that given a cell proper-length ℓ, it induces a working grid $\mathcal{G}^\ell$ and, in a natural way, the subcatalog creation process assure that all events placed at the maximal distance ℓ are taken into account. Because of the long-range correlations, this interevent distances have a considerable effect on the renormalized earthquake distributions. This fact is connected with distance declustering as proposed by Baiesi and Paczuski (2004), which take us directly to the second consequence: 2) The subcatalog creation process induce a time reordering. The idea of foreshock, mainshock and aftershock is explicitly defined. These temporal concepts have meaning only when a proper scale ℓ is previously given. One event might be aftershock or foreshock only at a fixed proper scale ℓ at a given cell belonging to a given grid, thus the long-range interevent-distances influences the long-range interevent-times. This is a general feature observed in various materials subjected to different mechanisms when thresholds are applied, see Janićević et al. (2016) for recent theoretical and experimental research.

Magnitude cutoff. The completeness of an earthquake point-catalog, that is the lower magnitude cutoff assuring a Gutenberg-Richter law, is related to the dimensionless moment Π_{M_0}. There is no unique cutoff assessment-procedure (Mignan & Woessner, 2012) because an independent relationship is needed. The parameter estimation used here is an alternative and it must be pursued in future works. No general micro-physical earthquake model can satisfactorily account for our fixed-point renormalized iteration, therefore no clear resolution is given here.

Homogeneity and isotropy. Other earthquake point-catalog characteristics that should be explored, in the proposed context, is dependence with respect to space-translation and

grid-azimuth of the renormalized event number Π^*, this is a delicate issue because our implicit notion of statistical homogeneity is only local, at the cell-grid level. Same thing can be said with regards to isotropy. In close relation to space-translation is depth dependence. As our grid analysis is bidimensional, all depth variations are lost, so various tectonic features are not incorporated. Future analysis should deal with these shortcomings.

Seismic cycle. The notion of seismic cycle has a proper-length scale attached to it, naturally the largest scale is intensely studied because it determines the maximum credible earthquake, a relevant notion in hazard studies. For example, on the western edge of the Andes, between 18 and 24°S latitude Métois et al. (2013) have established a series of segments, whose proper-lengths are believed to have some predictive power when analyzing the geodetic coupling. Similarly between 26 and 30°S latitude, there is a well known segment, quiescent since the 1922 *Mw* 8.6 earthquake (Ruiz & Madariaga, 2018). These segments, approximately 500 km, are associated with return periods ca. 100 years therefore it is natural to inquire about the relevance of the earthquake point-catalog studied, which covers a region from 18 to 45° S latitude and only 3 years long. The key idea is renormalization, i.e. the process by which the governing parameters are rescaled by means of exponents obtained from the observations. This process respects the relationship that is believed to exist between the segments (a proper-length scale), the seismic gap (a proper-time scale) and the magnitude of the earthquake that is expected in the gap (a proper-size scale) by extending this relationship to the whole data in the catalog, thus the gridding technique comprehensively covers the observable proper lengths, influencing the interevent times and seismic moment distributions, resulting in stable catalog properties such as those observed in Figure 6. Take for example events in cells ca. 333 km represented by circles and those cells ca. 999 km shown as stars. Although most circles and stars are at the right edge of Figure 6, at high Π_Q^* values, it is also true that there is mixing, this phenomenon is due to the collapse/renormalization process which induces a rearrangement when compared to Figure 5, where starts and circles are not mixed. It follows that inferences on the boundaries of Π_Q^* have been influenced by data in the other scales, i.e. there is an uncertainty reduction, especially where errors by extrapolation occur.

Tectonics. The average exponent values correspond to $p = 1.09$, $b_{\mathrm{GR}} = 0.99$, and $d_{\mathrm{BC}} = -1.97$, that is the renormalized event number represent a seismic moment release distribution with decaying (near) hyperbolic interevent times and lacunar-set support, denser than a Koch curve. Therefore, as indicated by Carpinteri and Chiaia (1997), the 2015-2017 Southern Andes situation is one of loading. By the time of the 1995 *Mw* 8.5 Antofagasta earthquake, Sobiesiak (2000) reported $b_{\mathrm{GR}} = 0.73$ over the fault plane with peaks at 0.54 and 1.08. Pastén and Comte (2014) gave a multifractal series converging to $d_\infty = 1.45$, so our values are higher on average, however those numbers have a local character. A recent global survey by Nishikawa and Ide (2014) reports b_{GR} values at six sections located between 19.8°S and 34.2°S latitude. Peaks range from $b_{\mathrm{GR}} = 0.79$ to 0.94 with a decreasing north-south trend. These values are in good accord with our findings. Finally Poulos et al. (2019) gives values between $b_{\mathrm{BR}} = 0.87$ and $b_{\mathrm{GR}} = 1.04$ for theirs zones 1 and 5, which are also consistent with our findings. More important is the physical significance of the joint scaling spanning ten orders of magnitude hinting at a *grand* process taking place from cortical mega-scale down to single-fault meso-scale.

Cascade of energy. Clearly, no energy transfer process is at play when passing from one proper scale to another. This scenario is analog to the cascade mechanism in turbulence (Batchelor, 1947) where vortices are created (or destroyed) without energy loss as long as the fluid is confined in an *inertial range* where vortices are small compared to the fluid proper-length scale. The inertial range in turbulence is a region delimited by two length boundaries: First, a lower limit such that viscous dissipation processes takes place on smaller scales and second, an upper limit such that forcing processes take place

on larger scales. The energy transfer process between this scales is characterized by a viscous-free energy rate dissipation spectra decaying as $\ell^{-5/3}$ (Kolmogórov, 1941). If the analogy stands, there must be a physical scale λ where earthquake source micro-processes taking place at scales smaller than λ might be considered stationary, so that no seismic-moment transfer mechanism takes place when going up to scales larger than λ. In other words, as long as the first similarity hypothesis over Π_u is fulfilled, no seismic-moment is released when passing from one scale to another. Likewise, there must be a mechanical scale where seismic-moment transfer processes between scales ceases to be dissipation free. A larger scale $\Lambda = \sqrt[3]{Q/(\Delta\sigma T^{-1})} \simeq 300\,\mathrm{km}$ is a candidate, but further studies are needed. Note the relevance of the observation period, while Q is supposed constant (steady seismic-moment release rate hypothesis) and $\Delta\sigma$ is by large a stable property, T is a catalog property and until we reach very long observation periods, spanning various earthquake cycles the energy cascade upper boundary cannot be known with reasonable certainty.

Earthquake hazard. The renormalized event number Π^* distribution is a zeroth-order hazard estimator, in terms of probabilities, the most important issue is the explicit dependence of scales, not only length scales but also interevent times and magnitude scales, and more importantly the boundaries where incomplete similarity holds. Earthquake hazard is an explicit function of the power exponents as well, and most importantly of the given observation period T and tectonic setting —defined by the seismogenic thickness H, the seismic-moment release-rate Q and the mean stress-drop $\Delta\sigma$— thus no material property is involved, all parameters are functions of the particular region under study i.e. the available earthquake point-catalogs and the specific tectonic conditions. This general comment is consistent with common empirical practice in hazard science. Maybe the functional shape of Φ^* can be shared among different areas, but recent studies have shown that more complex structures are present when other variables are analyzed, like earthquake taxonomy where different scalings are observed when epicenter clusters are organized in clusters (C. Siegel, 2022; C. E. Siegel et al., 2022).

Acknowledgments

PT, CS, RM and JC acknowledge financial support from the Seismic Risk Program (PRS). We thanks IPOC collaboration affiliated institutions (German Research Center For Geosciences (GFZ), Germany; GEOSCOPE Program of Institut de Physique du Globe de Paris and C.N.R.S., France; Centro Sismológico Nacional (CSN) of Faculty of Physical and Mathematical Sciences of University of Chile; and Universidad Católica del Norte, Chile) GFZ German Research Centre For Geosciences and Institut Des Sciences De L'Univers-Centre National De La Recherche CNRS-INSU (2006); Barrientos (2018) for the seismic network maintenance that made this work possible.

Figures were made with GMT (Wessel et al., 2019) and Inkscape. Gridding technique was implemented with GRASS GIS (Neteler et al., 2012). Catalog analysis were made with Numpy (Harris et al., 2020).

Data availability: Original and processed data available at (Toledo et al., 2023).

References

Aki, K. (1967). Scaling law of seismic spectrum. *Journal of Geophysical Research*, *72*(4), 1217–1231.

Aki, K. (1972). Earthquake mechanism. *Tectonophysics*, *13*(1-4), 423–446.

Aki, K. (1981). A probabilistic synthesis of precursory phenomena. In *Earthquake prediction* (p. 566-574). American Geophysical Union (AGU). Retrieved from `https://agupubs.onlinelibrary.wiley.com/doi/abs/10.1029/ME004p0566` doi: https://doi.org/10.1029/ME004p0566

Aki, K. (1996). Scale dependence in earthquake phenomena and its relevance to earthquake prediction. *Proceedings of the National Academy of Sciences*, *93*(9), 3740–3747.

Allmann, B. P., & Shearer, P. M. (2009). Global variations of stress drop for moderate to large earthquakes. *Journal of Geophysical Research: Solid Earth (1978–2012)*, *114*(B1).

Angermann, D., Klotz, J., & Reigber, C. (1999). Space-geodetic estimation of the Nazca-South America Euler vector. *Earth and Planetary Science Letters*, *171*(3), 329–334.

Baiesi, M., & Paczuski, M. (2004). Scale-free networks of earthquakes and aftershocks. *Physical review E*, *69*(6), 066106.

Bak, P., Christensen, K., Danon, L., & Scanlon, T. (2002). Unified scaling law for earthquakes. *Physical Review Letters*, *88*(17), 178501.

Barenblatt, G. I. (1987). *Dimensional analysis*. CRC Press.

Barenblatt, G. I. (2003). *Scaling*. Cambridge University Press. doi: 10.1017/CBO9780511814921

Barrientos, S. (2018). The seismic network of Chile. *Seismological Research Letters*, *89*(2A), 467–474.

Batchelor, G. (1947). Kolmogoroff's theory of locally isotropic turbulence. In *Mathematical proceedings of the cambridge philosophical society* (Vol. 43, pp. 533–559).

Benzi, R., Castaldi, I., Toschi, F., & Trampert, J. (2022). Self-similar properties of avalanche statistics in a simple turbulent model. *Philosophical Transactions of the Royal Society A: Mathematical, Physical and Engineering Sciences*, *380*(2218), 20210074. Retrieved from `https://royalsocietypublishing.org/doi/abs/10.1098/rsta.2021.0074` doi: 10.1098/rsta.2021.0074

Branch, M.-A., Coleman, T., & Li, Y. (1999). A subspace, interior, and conjugate gradient method for large-scale bound-constrained minimization problems. *SIAM Journal on Scientific Computing*, *21*(1), 1–23.

Camus, P., Arenas, F., Lagos, M., & Romero, A. (2016). Visión histórica de la respuesta a las amenazas naturales en Chile y oportunidades de gestión del riesgo de desastre. *Revista de Geografía Norte Grande*(64), 9–20.

Carpinteri, A., & Chiaia, B. (1997). Multifractal scaling laws in the breaking behaviour of disordered materials. *Chaos, Solitons & Fractals*, *8*(2), 135–150.

Christensen, K., Danon, L., Scanlon, T., & Bak, P. (2002). Unified scaling law for earthquakes. *Proceedings of the National Academy of Sciences*, *99*(suppl 1), 2509–2513.

Cisternas, M., Torrejón, F., & Gorigoitía, N. (2012). Amending and complicating Chile's seismic catalog with the Santiago earthquake of 7 august 1580. *Journal of South American Earth Sciences*, *33*(1), 102–109.

Contreras-Reyes, E., Jara, J., Grevemeyer, I., Ruiz, S., & Carrizo, D. (2012). Abrupt change in the dip of the subducting plate beneath north Chile. *Nature Geoscience*, *5*(5), 342.

Corral, A. (2003). Local distributions and rate fluctuations in a unified scaling law for earthquakes. *Physical Review E*, *68*(3), 035102.

Corral, A. (2005). Renormalization-group transformations and correlations of seismicity. *Physical review letters*, *95*(2), 028501.

Delouis, B. (2014). FMNEAR: Determination of focal mechanism and first estimate of rupture directivity using near-source records and a linear distribution of point sources. *Bulletin of the Seismological Society of America*, *104*(3), 1479–1500.

Derode, B., Delouis, B., & Campos, J. (2019). Systematic Determination of Focal Mechanisms over a Wide Magnitude Range: Insights from the Real-Time FMNEAR Implementation in Chile from 2015 to 2017. *Seismological Research Letters*, *90*(3), 1285–1295.

Diaconis, P., & Efron, B. (1983). Computer-intensive methods in statistics. *Scientific American*, *248*(5), 116–131.

Efron, B., & Tibshirani, R. J. (1994). *An introduction to the bootstrap*. CRC press.

Feder, J. (2013). *Fractals*. Springer Science & Business Media.

GFZ German Research Centre For Geosciences, & Institut Des Sciences De L'Univers-Centre National De La Recherche CNRS-INSU. (2006). *Ipoc seismic network*. Integrated Plate boundary Observatory Chile - IPOC. Retrieved from `http://geofon.gfz-potsdam.de/doi/network/CX` doi: 10.14470/PK615318

Goldenfeld, N. D. (1992). *Lectures on phase transitions and the renormalization group*. Addison-Wesley.

Goldstein, M. L., Morris, S. A., & Yen, G. G. (2004). Problems with fitting to the power-law distribution. *The European Physical Journal B-Condensed Matter and Complex Systems*, *41*(2), 255–258.

Golitsyn, G. S. (2001). Place of the Gutenberg-Richter law among other statistical laws of nature. *Vychislitel'naya Seysmologiya*, *32*, 119–137.

Golitsyn, G. S. (2007). Energy cycle of geodynamics and the seismic process. *Izvestiya, Physics of the Solid Earth*, *43*(6), 443–446.

Gutenberg, B., & Richter, C. F. (1956). Earthquake magnitude, intensity, energy, and acceleration: (second paper). *Bulletin of the seismological society of America*, *46*(2), 105–145.

Harris, C. R., Millman, K. J., van der Walt, S. J., Gommers, R., Virtanen, P., Cournapeau, D., ... Oliphant, T. E. (2020, September). Array programming with NumPy. *Nature*, *585*(7825), 357–362. Retrieved from `https://doi.org/10.1038/s41586-020-2649-2` doi: 10.1038/s41586-020-2649-2

Houdayer, J., & Hartmann, A. K. (2004). Low-temperature behavior of two-dimensional Gaussian Ising spin glasses. *Physical Review B*, *70*(1), 014418.

Huilgol, R. R., & Phan-Thien, N. (1997). *Fluid mechanics of viscoelasticity: general principles, constitutive modelling, analytical and numerical techniques*. Elsevier.

Janićević, S., Laurson, L., Måløy, K. J., Santucci, S., & Alava, M. J. (2016). Interevent correlations from avalanches hiding below the detection threshold. *Physical review letters*, *117*(23), 230601.

Kadanoff, L. P. (1966). Scaling laws for Ising models near T_c. *Physics Physique Fizika*, *2*(6), 263.

Kagan, Y. Y. (1994). Observational evidence for earthquakes as a nonlinear dynamic process. *Physica D: Nonlinear Phenomena*, *77*(1), 160–192.

Kagan, Y. Y., & Knopoff, L. (1980). Spatial distribution of earthquakes: the two-point correlation function. *Geophysical Journal International*, *62*(2), 303–320.

Kanamori, H., & Anderson, D. L. (1975). Theoretical basis of some empirical relations in seismology. *Bulletin of the seismological society of America*, *65*(5), 1073–1095.

Kolmogórov, A. (1941). Dissipation of energy in locally isotropic turbulence. In *Doklady akademii nauk* (Vol. 32, pp. 16–18).

Kossobokov, V., & Mazhkenov, S. (1994). On similarity in the spatial distribution of seismicity. *Computational seismology and geodynamics*, *1*, 6–15.

Kostrov, V. (1974). Seismic moment and energy of earthquakes, and seismic flow of rock. *Physics of the Solid Earth*, *1*, 13–21.

Lomnitz, C. (1970). Major earthquakes and tsunamis in Chile during the period 1535 to 1955. *Geologische Rundschau*, *59*(3), 938–960.

Lomnitz, C. (2004). Major earthquakes of Chile: a historical survey, 1535-1960. *Seismological Research Letters*, *75*(3), 368–378.

Madariaga, R. (1979). On the relation between seismic moment and stress drop in the presence of stress and strength heterogeneity. *Journal of Geophysical Research: Solid Earth*, *84*(B5), 2243–2250.

Madariaga, R. (2020). Earthquake source theory. *Encyclopedia of Solid Earth Geophysics*, 1–5.

Mendecki, A. J. (1996). *Seismic monitoring in mines*. Springer Science & Business Media.

Métois, M., Socquet, A., Vigny, C., Carrizo, D., Peyrat, S., Delorme, A., ... Ortega, I. (2013). Revisiting the North Chile seismic gap segmentation using GPS-derived interseismic coupling. *Geophysical Journal International*, *194*(3), 1283–1294.

Mignan, A., & Woessner, J. (2012). Estimating the magnitude of completeness for earthquake catalogs. *Community Online Resource for Statistical Seismicity Analysis*, 1–45.

Mueller, C. S. (2019). Earthquake catalogs for the USGS national seismic hazard maps. *Seismological Research Letters*, *90*(1), 251–261.

Neteler, M., Bowman, M., Landa, M., & Metz, M. (2012). GRASS GIS: a multi-purpose Open Source GIS. *Environmental Modelling & Software*, *31*, 124–130. doi: 10.1016/j.envsoft.2011.11.014

Nishikawa, T., & Ide, S. (2014). Earthquake size distribution in subduction zones linked to slab buoyancy. *Nature Geoscience*, *7*(12), 904–908.

Norabuena, E., Leffler-Griffin, L., Mao, A., Dixon, T., Stein, S., Sacks, I. S., ... Ellis, M. (1998). Space Geodetic Observations of Nazca-South America Convergence Across the Central Andes. *Science*, *279*(5349), 358–362. Retrieved from `https://science.sciencemag.org/content/279/5349/358` doi: 10.1126/science.279.5349.358

Ogata, Y. (1988). Statistical models for earthquake occurrences and residual analysis for point processes. *Journal of the American Statistical association*, *83*(401), 9–27.

Okubo, P. G., & Aki, K. (1987). Fractal geometry in the San Andreas fault system. *Journal of Geophysical Research: Solid Earth (1978–2012)*, *92*(B1), 345–355.

Omori, F. (1894). On the after-shocks of earthquakes. *J. Coll. Sci., Imp. Univ., Japan*, *7*, 111–200.

Ott, E. (2002). *Chaos in dynamical systems*. Cambridge university press.

Pastén, D., & Comte, D. (2014). ultifractal analysis of three large earthquakes in Chile: Antofagasta 1995, Valparaiso 1985, and Maule 2010. *Journal of seismology*, *18*(4), 707–713.

Poulos, A., Monsalve, M., Zamora, N., & de la Llera, J. C. (2019). An updated recurrence model for chilean subduction seismicity and statistical validation of its Poisson nature. *Bulletin of the Seismological Society of America*, *109*(1), 66–74.

Ranero, C. R., von Huene, R., Weinrebe, W., & Reichert, C. (2006). Tectonic processes along the Chile convergent margin. In *The andes* (pp. 91–121). Springer.

Rapp, B. E. (2016). *Microfluidics: modeling, mechanics and mathematics*. William Andrew.

Ruiz, S., & Madariaga, R. (2018). Historical and recent large megathrust earthquakes in Chile. *Tectonophysics*, *733*, 37–56.

Scholz, C. H., & Aviles, C. A. (1986). The fractal geometry of faults and faulting. In *Earthquake source mechanics* (p. 147-155). American Geophysical Union (AGU). Retrieved from `https://agupubs.onlinelibrary.wiley.com/doi/abs/10.1029/GM037p0147` doi: 10.1029/GM037p0147

Sedov, L. I. (1993). *Similarity and dimensional methods in mechanics*. CRC press.

Serra, I., & Corral, Á. (2017). Deviation from power law of the global seismic moment distribution. *Scientific reports*, *7*(1), 1–8.

Siegel, C. (2022). *Propiedades de similaridad de catálogos de sismicidad en el contexto tectónico de subducción del Norte Grande de Chile (19° S y 24° S)* (Tesis para optar al grado de magíster en ciencias). Universidad de Chile.

Siegel, C. E., Toledo, P., Madariaga, R., & Campos, J. (2022). Scaling of waiting time distribution in northern chile. *ESS Open Archive*. Retrieved from 10.1002/essoar.10508115.3

Sobiesiak, M. M. (2000). Fault plane structure of the Antofagasta, Chile earthquake of 1995. *Geophysical research letters*, *27*(4), 577–580.

Toledo, P., Siegel, C., Derode, B., Madariaga, R., & Campos, J. (2023, January). *Earthquake Scaling Equations Under Small Strain, Steady Moment Release-Rate Conditions in Southern Andes from 2015 to 2017.* Zenodo. Retrieved from https://doi.org/10.5281/zenodo.7644746 doi: 10.5281/zenodo.7644746

Tsuboi, C. (1940). Isostasy and maximum earthquake energy. *Proceedings of the Imperial Academy*, *16*(9), 449–454.

Tsuboi, C. (1956). Earthquake energy, earthquake volume, aftershock area, and strength of the Earth's crust. *Journal of Physics of the Earth*, *4*(2), 63–66.

Udías, A., Madariaga, R., Buforn, E., Muñoz, D., & Ros, M. (2012). The large chilean historical earthquakes of 1647, 1657, 1730, and 1751 from contemporary documents. *Bulletin of the Seismological Society of America*, *102*(4), 1639–1653.

Utsu, T., Ogata, Y., & Matsu'ura, R. S. (1995). The centenary of the Omori formula for a decay law of aftershock activity. *Journal of Physics of the Earth*, *43*(1), 1–33.

Vargas, G., Klinger, Y., Rockwell, T., Forman, S., Rebolledo, S., Baize, S., ... Armijo, R. (2014). Probing large intraplate earthquakes at the west flank of the Andes. *Geology*, *42*(12), 1083–1086.

Virkar, Y., & Clauset, A. (2014). Power-law distributions in binned empirical data. *The Annals of Applied Statistics*, *8*(1), 90–119. Retrieved from http://www.jstor.org/stable/24521727

Wessel, P., Luis, J., Uieda, L., Scharroo, R., Wobbe, F., Smith, W., & Tian, D. (2019). The Generic Mapping Tools version 6. *Geochemistry, Geophysics, Geosystems*, *20*(11), 5556–5564.

Widom, B. (2009). Scaling laws. *Scholarpedia*, *4*(10), 9054. doi: 10.4249/scholarpedia.9054

Wilson, K. G. (1975). The renormalization group: Critical phenomena and the Kondo problem. *Reviews of modern physics*, *47*(4), 773.

Wilson, K. G. (1979). Problems in physics with many scales of length. *Scientific American*, *241*(2), 158–179.

Zel'dovich, J. B. (1956). The motion of a gas under the action of a short-term pressure shock. *Soviet Physics Acoustics*, *2*(1), 25–35.

Figure1.

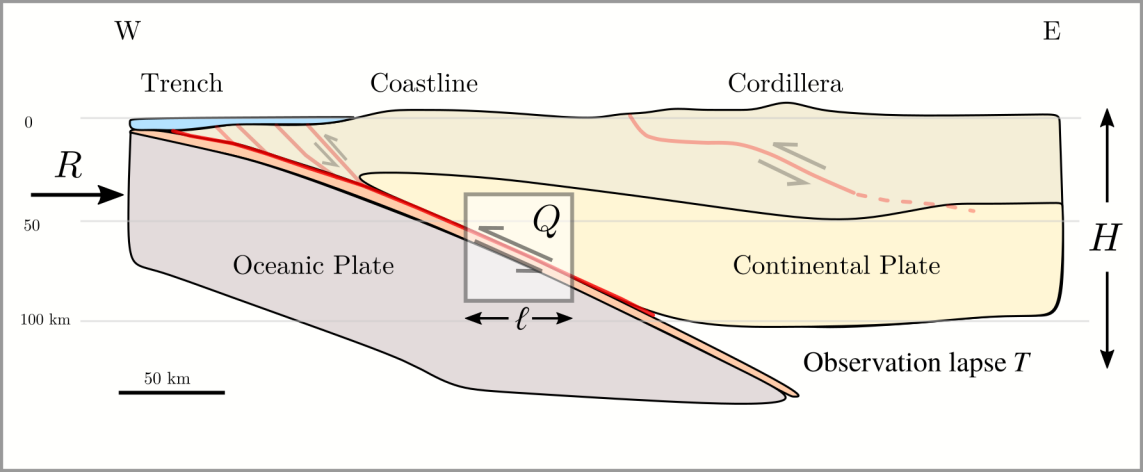
W
E
Trench
Coastline
Cordillera
0
R
50
Q
H
Oceanic Plate
Continental Plate
100 km
ℓ
Observation lapse T
50 km

Figure2.

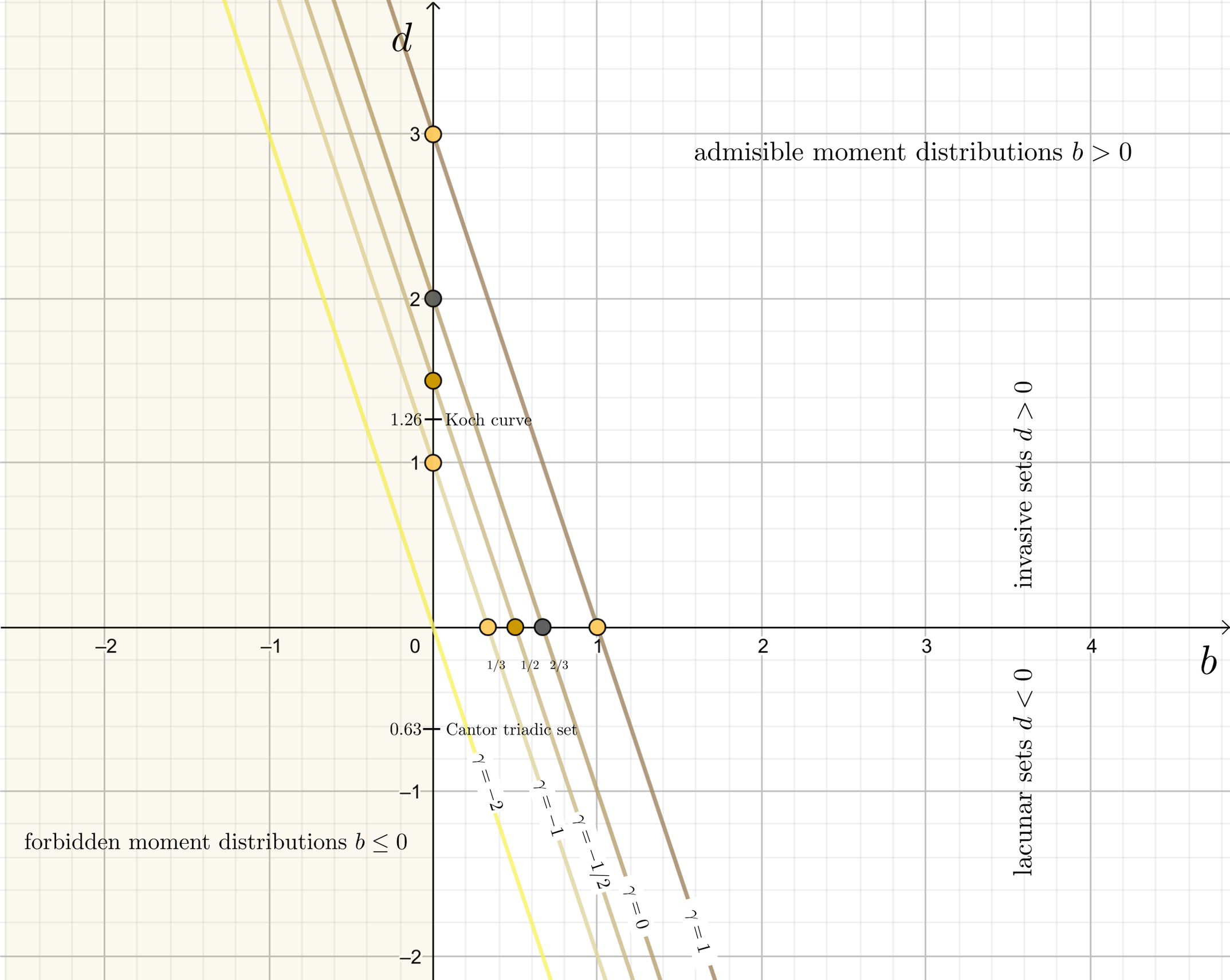
d
b
admisible moment distributions $b > 0$
invasive sets $d > 0$
lacunar sets $d < 0$
forbidden moment distributions $b \leq 0$
1.26 Koch curve
0.63 Cantor triadic set
1/3
1/2
2/3
$\lambda = -2$
$\lambda = -1$
$\lambda = -1/2$
$\lambda = 0$
$\lambda = 1$
3
2
1
0
−1
−2
−2
−1
1
2
3
4

Figure3.

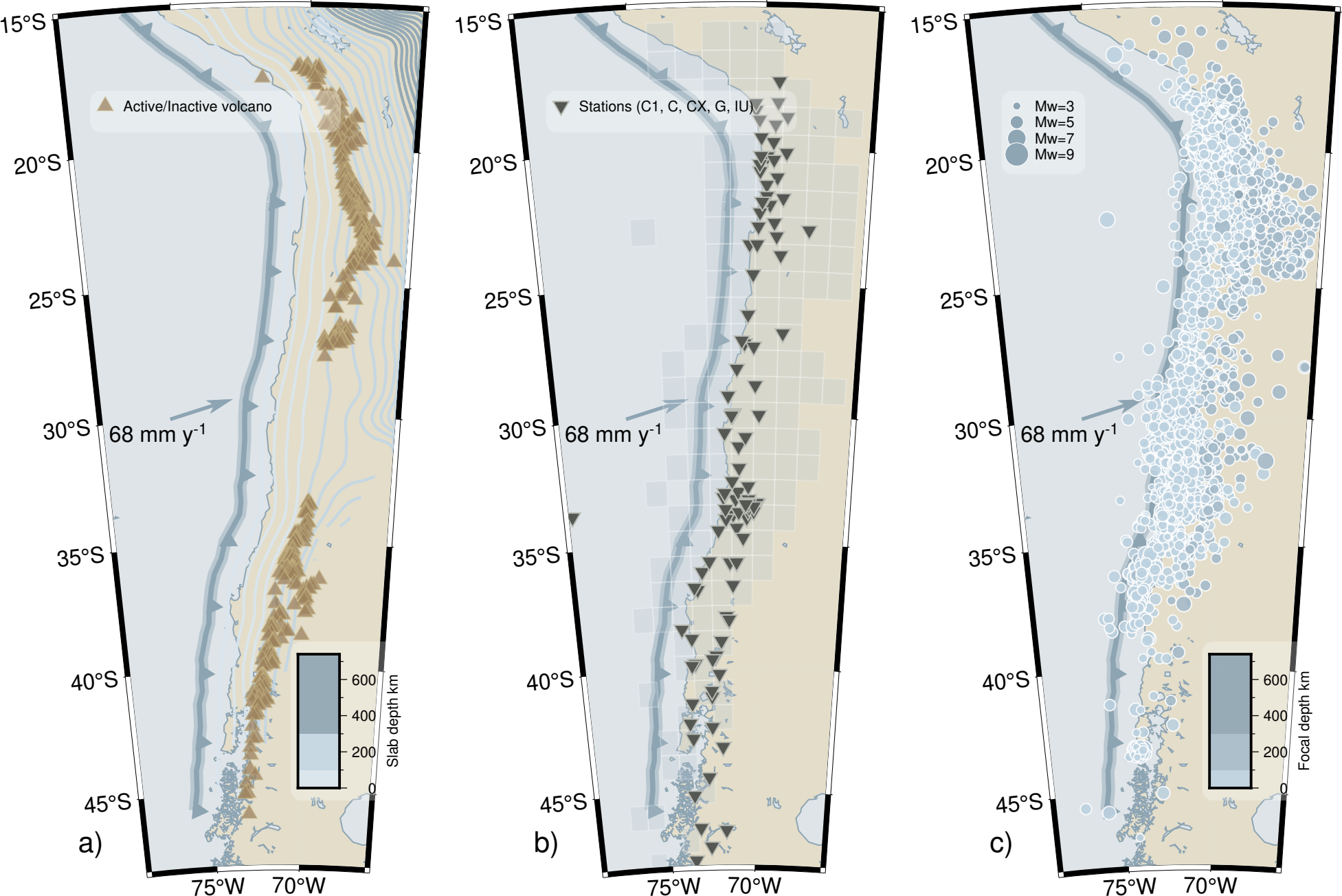
Active/Inactive volcano
68 mm y-1
Slab depth km
600
400
200
0
a)
Stations (C1, C, CX, G, IU)
68 mm y-1
b)
Mw=3
Mw=5
Mw=7
Mw=9
68 mm y-1
Focal depth km
600
400
200
0
c)
15°S
20°S
25°S
30°S
35°S
40°S
45°S
75°W
70°W

Figure4.

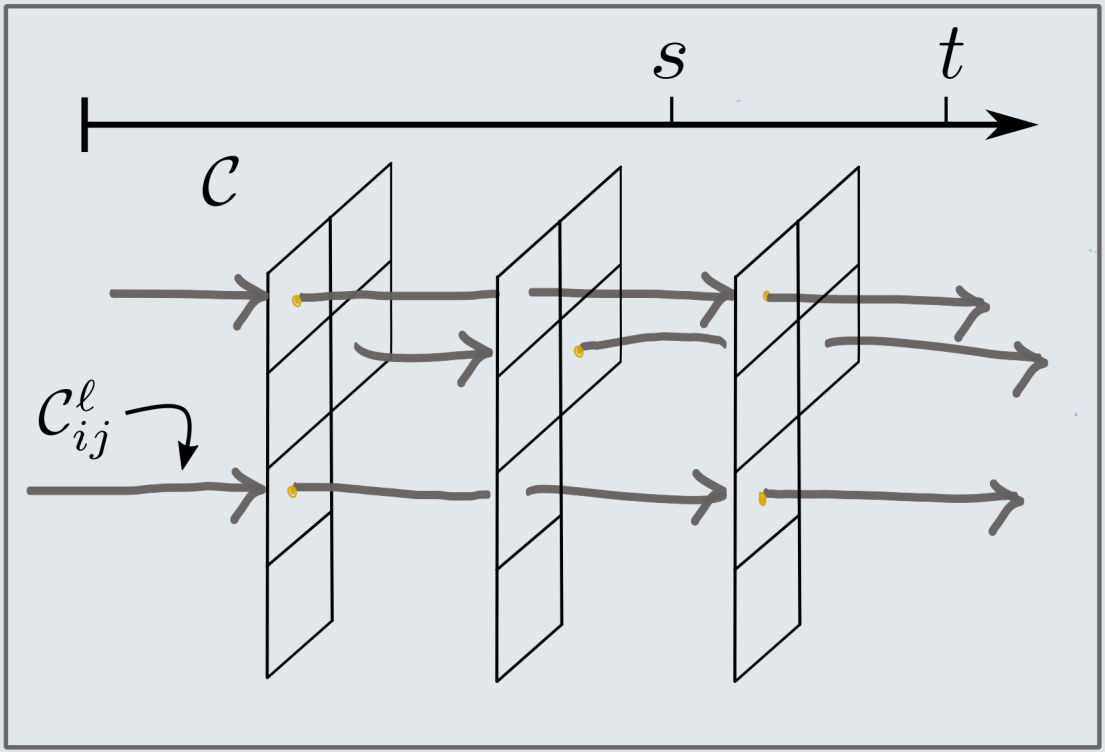
s
t
$\mathcal{C}$
$\mathcal{C}_{ij}^{\ell}$

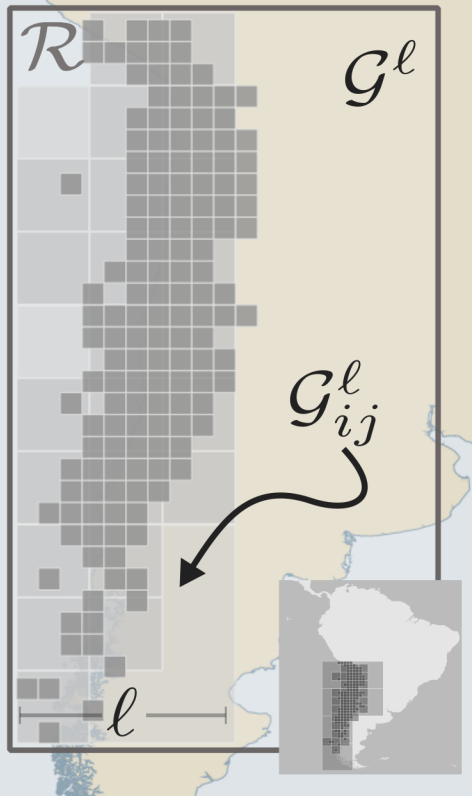
$\mathcal{R}$
$\mathcal{G}^{\ell}$
$\mathcal{G}_{ij}^{\ell}$
ℓ

Figure5.

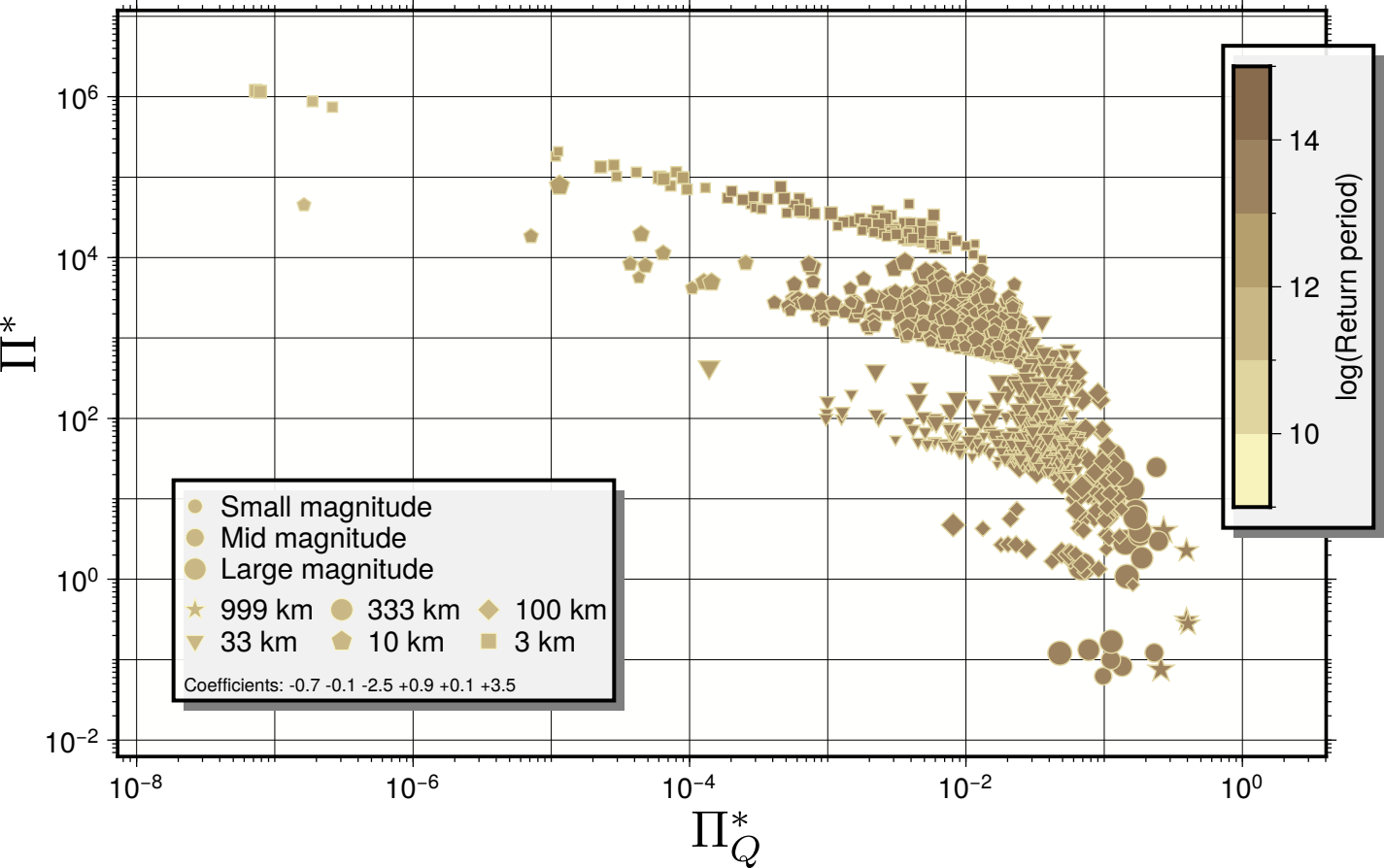
10^6
10^4
10^2
10^0
10^{-2}
Π^*
10^{-8}
10^{-6}
10^{-4}
10^{-2}
10^0
Π^*_Q
log(Return period)
14
12
10
Small magnitude
Mid magnitude
Large magnitude
999 km
333 km
100 km
33 km
10 km
3 km
Coefficients: -0.7 -0.1 -2.5 +0.9 +0.1 +3.5

Figure6.

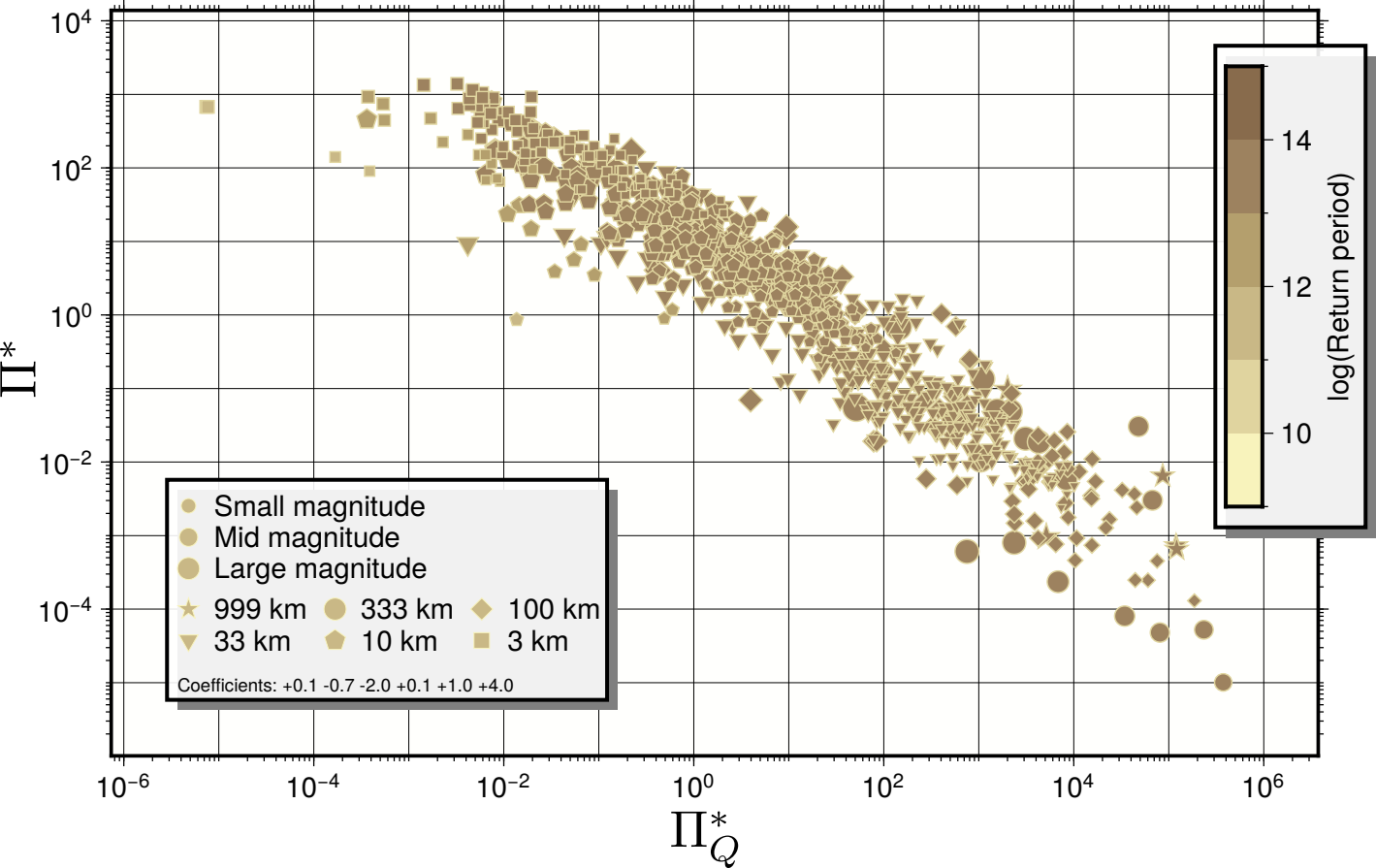
10^4
10^2
10^0
10^{-2}
10^{-4}
Π^*
10^{-6}
10^{-4}
10^{-2}
10^0
10^2
10^4
10^6
Π^*_Q
log(Return period)
14
12
10
Small magnitude
Mid magnitude
Large magnitude
999 km
333 km
100 km
33 km
10 km
3 km
Coefficients: +0.1 -0.7 -2.0 +0.1 +1.0 +4.0